Finanziato dall'Unione europea NextGenerationEU

Ministero dell'Università e della Ricerca

Global Stability of Road Vehicle Motion - STAVE

Deliverable 2
Bifurcation Theory Applied to Vehicle System Dynamics

Document in fulfilment of
MILESTONE 2
"Bifurcation analysis performed, taxonomy performed, Lyapunov analysis performed"

This project has received funding from Italian Ministero del Merito e della Ricerca, PRIN: Progetti di ricerca di rilevante interesse nazionale – Bando 2022 PNRR Prot. P2022KSN9Z

Table of Contents

Abstract 3
1. Vehicle-and-driver dynamics and Bifurcation Theory. 4
1.1 Any vehicle is made unstable by driver action for a sufficiently high forward velocity 4
1.2 Taxonomy of bifurcations that cause vehicle instability 5
1.3 Impact of drivers driving ability on vehicle instability 8
1.4 Impact of control systems on vehicle instability 8
2 Definition and computation of the threshold above which a disturbance cause instability 10
2.1 Region of Attraction (RoA) and the role of the saddle limit cycle 10
2.2 Formal definition of the limit of stability 10
2.3 Floquet theory for early detection of unstable motions [7] 11
2.3.1 Applicability of the DoS criterion 13
2.3.2 Selection of the point $z0$ on the limit cycle 14
2.3.3 Practical application 14
2.3.4 Interpretation of the stability index 15
Method to introduce Lyapunov functions into complex vehicle models 16
2.4 Formal definition of a Lyapunov function for vehicle dynamics 16
2.5 Sum Of Squares (SOS) methods to inner approximate of the stability region 17
3.Path tracking for motorsport and road vehicles 20
Conclusions 22
References 23

Abstract

This deliverable aims at establishing the basic concepts developed in STAVE that link Vehicle System Dynamics to Bifurcation Theory.

This document is organized as follows.

Section 1 describes how drivers create Hopf bifurcations, thus linking vehicle-and-driver dynamics to Bifurcation Theory. The influence of driver's ability and common controls like ESP on vehicle stability has been assessed.

Section 2 defines and computes the threshold above which a disturbance cause instability. Floquet theory for an early classification of stable and unstable motion is applied.

Section 3 describes a method to introduce Lyapunov functions into complex vehicle models. Section 3 introduces a technique developed to make an inner estimate, using Lyapunov functions, of the region of stability of the desired motion. The corresponding paper will be produced later.

Conclusions in Section 4.

1. Vehicle-and-driver dynamics and Bifurcation Theory.

After a severe lane change, a wind gust, or another disturbance, the driver might be unable to recover the intended motion. Even though this fact is known by any driver, the scientific investigation and testing on this phenomenon is just at its very beginning.

1.1 Any vehicle is made unstable by driver action for a sufficiently high forward velocity

The first step in our investigation was to identify the origin of vehicle instability. To this end, we coupled the simplest vehicle model (Model 1 from Deliverable 1) with the driver model introduced in the same document, resulting in a combined vehicle-and-driver system described by the following set of equations:

$$\begin{aligned}
\dot{v} &= \frac{1}{m}\left(F_{y_f} + F_{y_r} + F\right) - u\,r \\
\dot{r} &= \frac{1}{J}\left(a\,F_{y_f} - b\,F_{y_r} + M\right) \\
\dot{\delta} &= \delta_1 \\
\dot{\delta}_1 &= \delta_2 \\
\dot{\delta}_2 &= \frac{6}{\tau^3}\left(-\delta - \tau\,\delta_1 - \left(\frac{\tau^2}{2}\right)\delta_2 + k\,e + k_d\dot{e}\right) \\
\dot{y}_G &= v + u\,\psi \\
\dot{\psi} &= r
\end{aligned}$$

where v is the lateral speed, r is the yaw rate, δ is the steering angle, y_G is the lateral position, and ψ is the heading angle of the vehicle with respect to the reference path—together defining the path error (see Section 2 of Deliverable 1).

$$\begin{aligned}
e &= \left(y_{ref} - y_P\right) = -y_P = y_G - L\sin\psi \\
\dot{e} &= \left(\dot{y}_{ref} - \dot{y}_P\right) = -\dot{y}_P
\end{aligned}$$

since the reference path is assumed to be straight and aligned with the longitudinal axis of the vehicle.

Parameters a and b denote the distances from the center of mass to the front and rear axles, respectively. m is the vehicle mass, and J its inertia momentum, while u is the constant forward velocity. The lateral tire forces F_{y_f} and F_{y_r} (see Section 1 of Deliverable 1) represent the interaction between tires and road, and can be computed using the Pacejika magic formula [1] as

$$F_{y_i}(\alpha_i) = D_i \sin\left(C_i \arctan\left(B_i\alpha_i - E_i(B_i\alpha_i - \arctan(B_i\alpha_i))\right)\right), i = f, r,$$
$$\alpha_f = \delta - \left(\frac{v + ra}{u}\right), \alpha_r = -\left(\frac{v - rb}{u}\right)$$

The driver model includes a response delay τ, a feedback gain k, and an anticipatory gain k_d. External disturbances are modeled as force F and torque M.

We analyzed this model by varying system parameters, focusing on the driver's ability to maintain a straight trajectory. Mathematically, this corresponds to analyzing the stability of the equilibrium $x = \left(v, r, \delta, \dot{\delta}, \ddot{\delta}, y_G, \psi\right) = 0$.

To study local stability, the system is linearized around this equilibrium. The resulting linear system is:

$$\dot{\delta x} = J\,\delta x,$$

where δx is the state deviation and J is the Jacobian matrix evaluated at the origin, that is

$$J = \begin{bmatrix} -\frac{F_f+F_r}{mu} & -\frac{aF_f-bF_r+mu^2}{mu} & 0 & 0 & \frac{F_f}{m} & 0 & 0 \\ -\frac{aF_f-bF_r}{Ju} & -\frac{aF_f-bF_r}{Ju} & 0 & 0 & a\frac{F_f}{J} & 0 & 0 \\ -\frac{6}{\tau^3}k_d & -\frac{6}{\tau^3}k_d L & -\frac{3}{\tau} & -\frac{6}{\tau^2} & -\frac{6}{\tau^3} & -\frac{6}{\tau^3}k & -\frac{6u(kT_{prev}+k_d)}{\tau^3} \\ 0 & 0 & 1 & 0 & 0 & 0 & 0 \\ 0 & 0 & 0 & 1 & 0 & 0 & 0 \\ 1 & 0 & 0 & 0 & 0 & 0 & u \\ 0 & 1 & 0 & 0 & 0 & 0 & 0 \end{bmatrix}$$

where $F_i = B_i C_i D_i,\ i = f, r$. The linear analysis shows that at low forward velocities u, the system is asymptotically stable (i.e., all eigenvalues of J have negative real parts). As u increases, a pair of complex-conjugate eigenvalues crosses the imaginary axis, indicating the onset of instability through a Hopf bifurcation **Errore. L'origine riferimento non è stata trovata.**.

It is well known that oversteering vehicles tend to become unstable at high speed, whereas understeering vehicles are traditionally considered stable at any speed when the driver is not modeled. Our analysis demonstrates that once the driver is included, **any vehicle—understeering or oversteering—becomes unstable beyond a certain forward velocity [3]**. This result provides a rigorous mathematical explanation for a widely acknowledged empirical fact: **every vehicle becomes unmanageable at high enough speeds due to the limitations in driver response.**

1.2 Taxonomy of bifurcations that cause vehicle instability

The analysis performed allows us to go further: in fact, by examining how the desired mode of operation loses its stability properties, we can understand which other system invariants are involved. The scenario presented corresponds to a **Hopf bifurcation**. The analysis of the nonlinear terms shows that, in this bifurcation, a **limit cycle** is involved, which at the moment of the bifurcation collides with the desired equilibrium, changing its stability properties. In particular, two scenarios are possible **Errore. L'origine riferimento non è stata trovata.**:

- **Subcritical Hopf bifurcation**: where an unstable limit cycle collides with the stable equilibrium, altering its stability properties (Figure 1, panel a);
- **Supercritical Hopf bifurcation**: where a stable limit cycle is born around the equilibrium when it becomes unstable (Figure 1, panel b), generating oscillations of increasing amplitude.

These two scenarios are often classified as **catastrophic** (subcritical Hopf) and **non-catastrophic** (supercritical Hopf), because as the parameter varies, in the catastrophic case there is no attractor in the neighborhood after the bifurcation. Therefore, after the bifurcation, a small perturbation causes a large transient that moves the system away from the previously stable operating mode. In the non-catastrophic case, an attractor emerges nearby after the bifurcation, so a small perturbation sets the system to operate in a mode not too different (small oscillations around the reference trajectory, in our case) from the desired one.

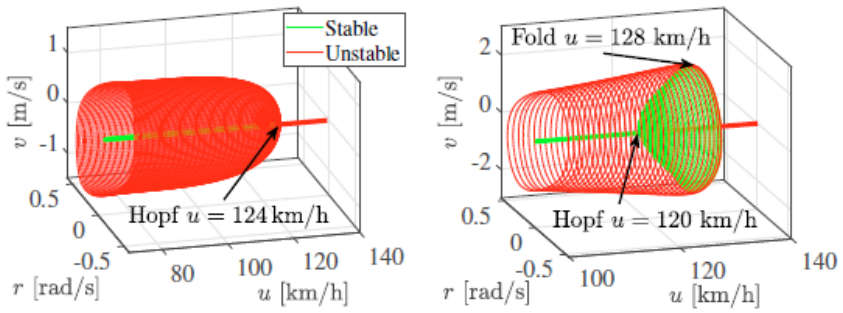

(a) $k_d = 0.004$ (b) $k_d = 0.006$

Figure 1: Bifurcation diagram of the model under analysis. The projection of the invariant (either equilibria of limit cycles) as function of vehicle forward velocity on the (v, r) plane are reported in red when unstable, in green when stable.

Both cases are possible in our model, as shown in the figure, and the transition from one case to the other depends on vehicle and driver parameters. For example, Figure 1 shows that a low driver anticipation capacity is typically associated with the subcritical Hopf bifurcation, while a driver with higher anticipation capacity will encounter a supercritical Hopf bifurcation.

It is interesting to note that since both cases are possible, the system can transition from one to the other as parameters vary: the transition from subcritical to supercritical Hopf is itself a bifurcation, called a **codimension-2 bifurcation**, known as the **Bautin bifurcation** or **Generalized Hopf** bifurcation **Errore. L'origine riferimento non è stata trovata.**. This bifurcation also involves a **fold bifurcation of limit cycles**. This tells us that even in the best case (the non-catastrophic one), the stable limit cycle generated as forward velocity increases will collide and disappear with a **saddle limit cycle**: thus, for velocities at which the vehicle-plus-driver system can still follow the reference trajectory (i.e., forward velocities lower than the Hopf bifurcation velocity), a saddle limit cycle is present.

The presence of an unstable limit cycle delimiting the basin of attraction of the desired motion has been analyzed using the driving simulator facility available at Politecnico di Milano (see Figure 2) [4].

Figure 3 reports the v and r measurements for four trajectories (obtained with two different vehicle setups) recorded in the driving simulator: two of them (green) correspond to cases where the driver was able to recover straight motion, and two (red) led to the end of the simulation, resulting from different initial perturbations. As one can see, the trajectories describe a cyclical path before converging or diverging.

Physical quantity	Values
Platform size	6m x 6m
Visual system (H)	270°
Visual system (V)	45°
Degrees of freedom	9
Longitudinal acceleration	1.5g
Vertical acceleration	2.5g
Lateral acceleration	1.5g
Lateral travel	4.2m
Longitudinal travel	4.2m
Vertical travel	± 298mm
Yaw angle	± 62°
Pitch angle	± 15°
Roll angle	± 15°

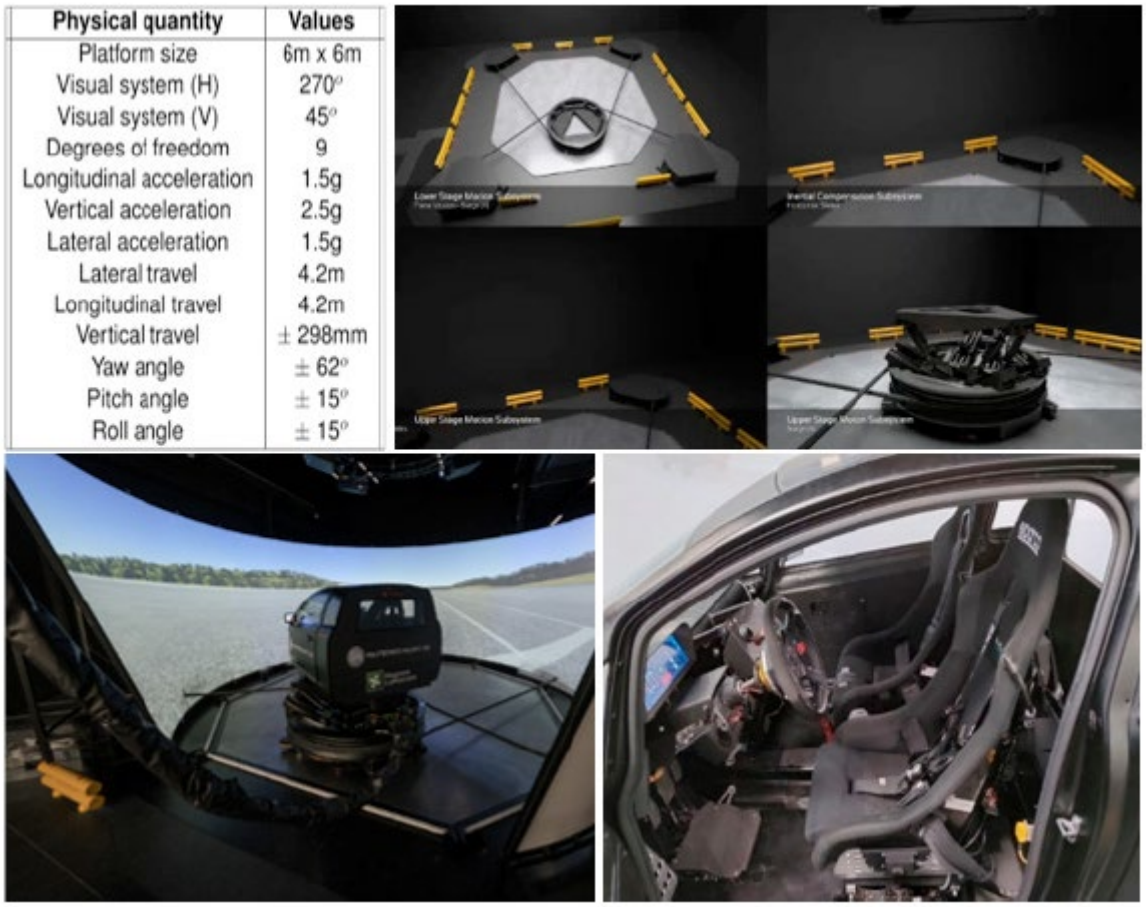

Figure 2: Dynamic driving simulator of the Politecnico di Milano - www.drismi.polimi.it

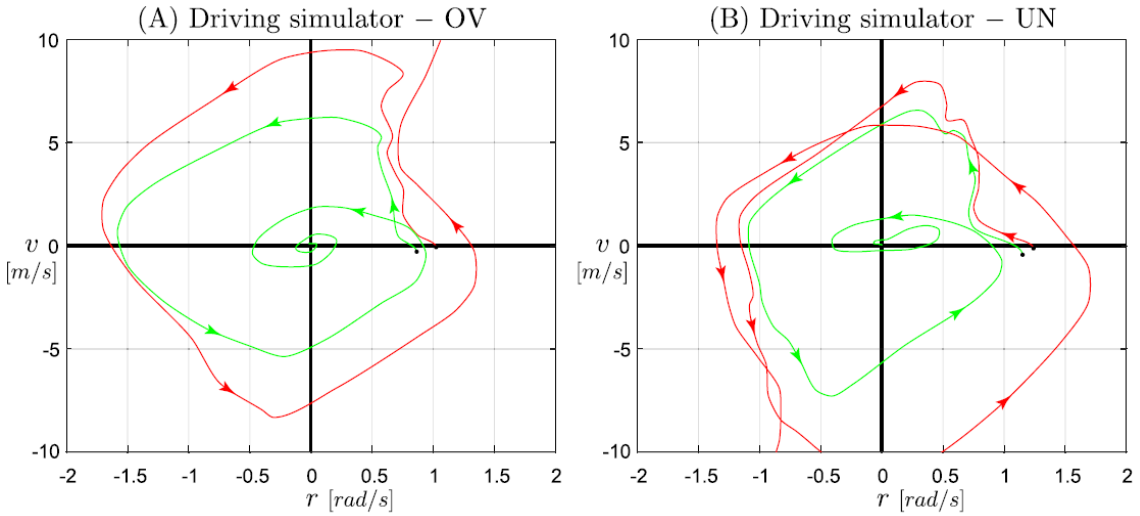

Figure 3: Projection of two trajectories in the (v,r)-plane, obtained with the complex vehicle model controlled by a human driver at the driving simulator for the oversteering (left panels) and the understeering (right panels) vehicle configuration (see Deliverable 1). Forward speed $u = 90$ km/h.

1.3 Impact of drivers driving ability on vehicle instability

As previously discussed, the **main cause of instability lies in the driver's reaction time and response behavior**. Using bifurcation analysis, we investigated how the **instability threshold**—that is, the critical velocity at which a Hopf bifurcation occurs—as well as the **type of Hopf bifurcation**, change as a function of the driver's parameters: the reactivity k_p, the anticipation ability k_d, and the response delay τ. The results are illustrated in Figure 4.

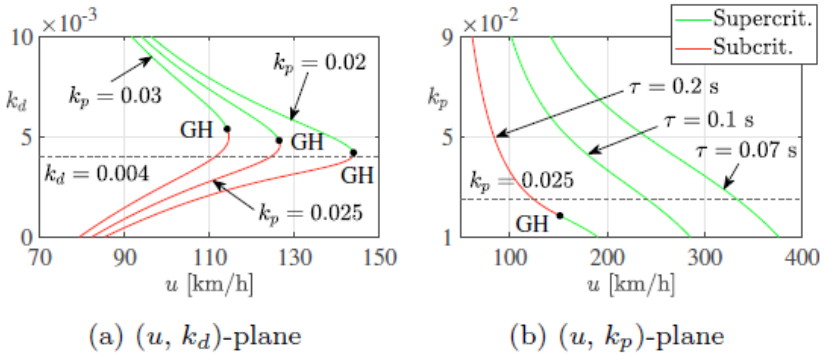

Figure 4: Hopf bifurcation curves for the model under analysis, in red or green when subcritical or supercritical, respectively.

The **Hopf bifurcation curves** shown in panel (a) clearly illustrate both the **transition between subcritical and supercritical regimes** (a Generalized Hopf or **Bautin bifurcation**, labeled "GH") and the existence of an **optimal value of** k_d, which depends on k_p, that **maximizes the critical velocity** (i.e., the steady-state becomes unstable when crossing the Hopf curve from left to right). Lower values of k_p correspond to higher critical velocities.

In panel (b), the Hopf curve is shown in the (u, k_p)-plane for three different values of the steering delay τ. As τ decreases, the **critical velocity increases dramatically**, and the Hopf bifurcation becomes **supercritical for any given value of** k_p. When $\tau \to 0$, the Hopf bifurcation disappears altogether: the **delay in the application of the steering command is the primary cause for the generation of limit cycles**.

The **unstable cycle** that characterizes the perturbed rectilinear motion of the vehicle-and-driver system is of the **saddle type**: in phase space, trajectories are temporarily attracted to the cycle, and then repelled—either towards the **stable equilibrium** or towards a **spin condition**.

1.4 Impact of control systems on vehicle instability

The control system architecture, schematized in Figure 5, and the controller dynamics has been derived in Deliverable 1 and are here briefly reported:

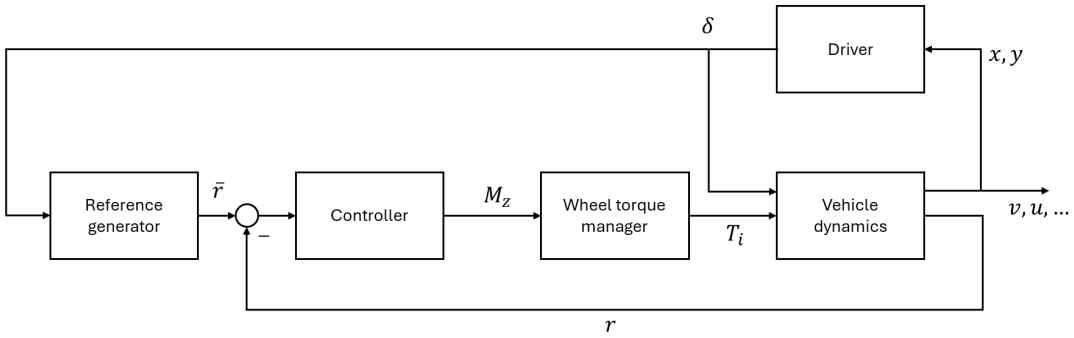

Figure 5: Control system architecture.

The reference generator module has been improved by adding saturations to the maximum imposable reference yaw rate $\bar{r}$, smoothed out for numerical reasons through the use of a hyperbolic tangent:

$$\bar{r} = \tanh\left(\frac{u\,\delta}{l + k_{us}u^2} \cdot \frac{1}{r_{max}}\right) r_{max};$$

$$r_{max} = \frac{g}{u} p.$$

Where p is a tuneable parameter that can be used to select a desired maximum reference yaw rate.

To determine the effects of the controller on the stability of the vehicle, a bifurcation analysis has been conducted over the simplified 2DOF single-track model presented in Deliverable 1, with the driver module removed and replaced by a time invariant steering angle δ, reported in Figure 6.

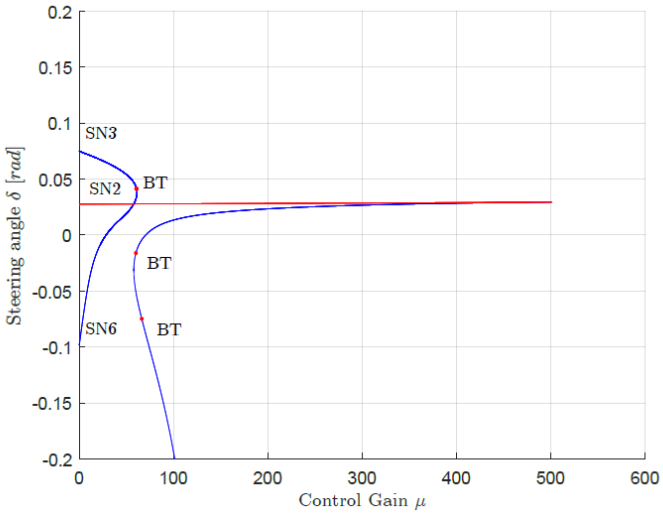

Figure 6: Bifurcation diagram in (δ, μ) with a fixed longitudinal velocity of u = 90 Km/h. Only half of the bifurcations are plotted for clarity purposes, the other half is symmetric with respect to the x-axis.

The causes of instability of the vehicle mounting the oversteering tires setup has been carefully explored, deriving an analytical way to define the minimum control gain value of the controller that guarantees stability μ_{min}. It is also shown a diminishing effect on the efficiency of the controller itself, leading to an analytical way to determine upper bound for the value of the control gain μ_{max} .

2 Definition and computation of the threshold above which a disturbance cause instability

2.1 Region of Attraction (RoA) and the role of the saddle limit cycle

We are now ready to mathematically explain why there are always disturbances (such as a **severe lane change**, a **wind gust**, etc.) that the driver is **unable to recover from** and restore the vehicle to the reference trajectory: the desired mode of operation is **not globally stable**, but instead possesses a **basin of attraction**, due to the presence of a **saddle-type limit cycle**.

Mathematically speaking, given a certain forward velocity, let us consider a disturbance acting on the vehicle body. If we model this disturbance as an **impulse** applied to the body via a **force** F and/or a **torque** M, the result is an initial state with **nonzero lateral velocity** v and **yaw rate** r, while all the other states remain at 0.

This can be justified as follows: if the external inputs F and M are modeled as Dirac delta functions, then the instantaneous values of $\dot{v}$ and $\dot{r}$ at the time of the impulse are different from 0. This is due to the specific structure of the governing equations, where F and M appear only in the differential equations for $\dot{v}$ and $\dot{r}$.

The **saddle limit cycles** shown in Figure 1 therefore cause the **existence of a basin of attraction**, as they partitions the state space into two non-negligible regions: one containing trajectories that converge to the desired motion, and the other containing trajectories that diverge—delimited by the **(N−1)-dimensional surface** formed by trajectories that converge to the saddle limit cycle itself. Importantly, as the amplitude of the limit cycle grows as we diminish the forward speed, the **initial conditions that lead to instability are larger at low forward speeds**, which aligns with physical intuition: larger deviations correspond to stronger disturbances.

The $\mathbb{R}^{N-1}$ dimensional surface containing all the initial conditions that converge to the saddle limit cycle is called the **stable manifold of the saddle limit cycle**, and it has **measure zero** in $\mathbb{R}^N$. Initial conditions on one side of this manifold lead to recovery of the desired behavior, while those on the other side evolve away from it—and generate what is commonly interpreted as an **unstable motion**.

2.2 Formal definition of the limit of stability

Since disturbances affect only the initial conditions of the lateral velocity v and yaw rate r—as these are the only state variables they can instantly modify—the intersection of the stable manifold of the saddle limit cycle with the velocity–yaw-rate plane becomes particularly relevant. We refer to this intersection as **ISMaVeR** (**I**ntersection of the **S**table **Ma**nifold with the **Ve**locity and **R**oll plane) [6].
The points inside ISMaVeR represent all initial conditions with $v \neq 0, r \neq 0$, and all other state variables set to zero—i.e., all initial conditions that can result from a disturbance—that lead to convergence towards the desired mode of operation. Conversely, the points outside ISMaVeR lead to diverging trajectories. In other words, ISMaVeR defines the set of disturbances that the vehicle-and-driver system is able to handle and recover from. Therefore, **the area of ISMaVeR can be interpreted as a measure of the system's robustness to external disturbances**.

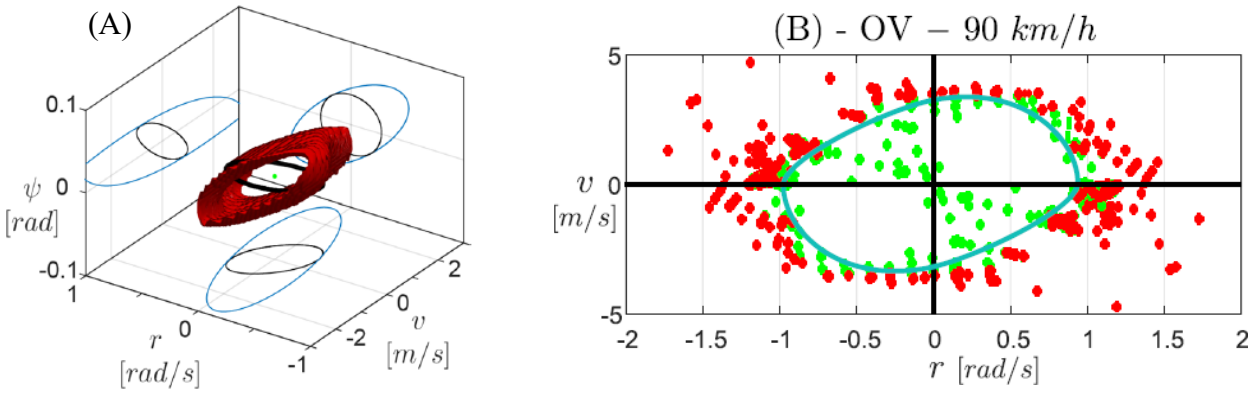

Figure 7: (A) Projection of the saddle-type limit cycle (black line) onto the (ψ, v, r) subspace at $u = 90\ km/h$. The red surface is the projection on the 3D subspace of the 6D stable manifold of the limit cycle, whose intersection with each plane is reported in blue, while the black closed curve is the projection of the limit cycle on each plane. The closed blue line on the (v, r) plane is called ISMaVeR and define the RoA of the desired behavior. (B) Comparison between the ISMaVeR computed with the model and the smallest initial conditions at the driving simulator which cause instability. Dots refer to initial conditions of the complex vehicle model driven -at the driving simulator- by a human driver. The dots are green if the driver can return to the desired path after the disturbance, red otherwise.

In Figure , we show the projection of the 6D stable manifold of the saddle limit cycle onto a 3D subspace. The intersections with the coordinate planes are shown in blue, while the black closed curve represents the projection of the limit cycle on each plane for the OV vehicle configuration (see Deliverable 1 for model parameters). The closed blue curves in the (v, r)-plane are what we refer to as ISMaVeR, and they define the basin of attraction of the controlled equilibrium after a disturbance (i.e. under the assumption $\psi(0) = y_G(0) = \delta(0) = \delta_1(0) = \delta_2(0) = 0$). On the right side of the figure, the same ISMaVeR curve is displayed, overlaid with a scatter plot of green and red dots representing initial conditions of the full vehicle model driven by a human driver in the driving simulator. The green dots indicate successful recovery (the driver returns to the reference trajectory), while the red dots indicate failure (the driver cannot recover). This experimental validation confirms that the results obtained via mathematical analysis of the model have quantitative predictive power.

2.3 Floquet theory for early detection of unstable motions [7]

Having shown that the possible loss of vehicle control is directly linked to the existence of a saddle-type limit cycle, we have proposed a novel methodology for vehicle stability sensing based on the mathematical analysis of trajectories near the saddle cycle. The goal is to define a precise criterion to recognize—immediately after a disturbance—whether the driver will ultimately be able to recover the steady-state condition. To explain the rationale behind the method, we first present an example of a two-dimensional system, with a stable equilibrium and a saddle, whose phase portrait is shown in Figure . The system has two equilibria: a saddle point z_0 and a stable node z_E. The stable manifold of the saddle divides the phase plane into two distinct regions: initial conditions on one side lead to convergence toward z_E, while those on the other side diverge. The geometry of the stable and unstable manifolds is closely related to the

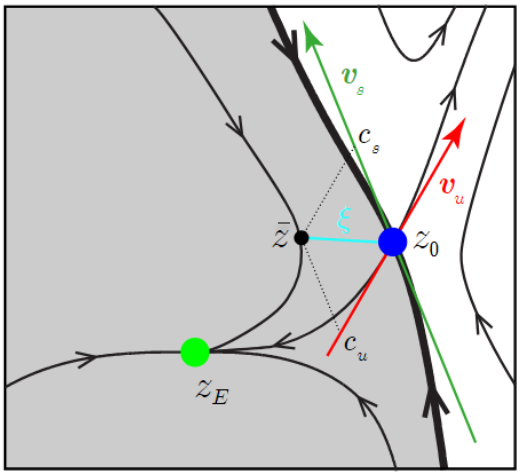

Figure 8: Phase portrait of a 2D system in the neighborhood of a saddle equilibrium z_0. The eigenvectors of the system linearized at the saddle are highlighted (v_s: stable, v_u: unstable); they are tangent to the corresponding manifolds at the saddle. The basin of attraction of the stable node z_E, shaded, is delimited by the stable manifold of the saddle (thicker trajectory): a trajectory from any initial state $\bar{z}$ converges to z_E only if it is on the left side of the stable manifold.

eigenvectors of the system linearized at the saddle. These eigenvectors, denoted v_s (stable) and v_u (unstable), are tangent to their respective manifolds at z_0, and define a local basis of the phase space.

Given any state $\bar{z}$, its relative position with respect to the saddle can be assessed by expressing the deviation $\xi = \bar{z} - z_0$ in the eigenbasis:

$$\xi = c_s v_s + c_u v_u$$

The sign of the coefficient c_u determines on which side of the stable manifold the point lies. If $c_u < 0$, the trajectory starting at $\bar{z}$ is expected to diverge, lying on the 'wrong' side of the manifold.

This reasoning can be extended for the analysis of the basin of attraction of an equilibrium in $\mathbb{R}^N$ in the case where the basin of attraction is delimited by the $\mathbb{R}^{N-1}$-stable manifold of a **saddle limit cycle**, as in the common case of a cycle emerging from a subcritical Hopf bifurcation. To make the idea more intuitive, we make this extension in a 3D example, assuming therefore that the stable and unstable manifolds of the saddle limit cycle are 2D. In this case, the situation is the one reported in Figure .

As for the previous case, the saddle limit cycle is at the intersection of its stable and unstable manifolds, and one side of the unstable manifold converge to the equilibrium z_E. For a point $\bar{z}$ we can therefore compute the distance ξ from a suitable point of the saddle limit cycle, and therefore express it in the coordinate space of the stable and unstable manifolds. As for the previous case, to compute them we have to linearize the motion around the limit cycle: this can be done using Floquet theory by computing the so called limit cycle monodromy matrix, and use its eigenvectors computed in z_0 to express

$$\xi = \sum_{i=1}^{N} c_i v_i$$

where in the summation, to cope with the example in the figure, the three vectors needed to express ξ are the red and green vectors v_u and v_s, that are associated to the unstable eigenvalue k_u and the stable eigenvalue k_s the monodromy matrix respectively (the eigenvalue of the monodromy matrix are called Floquet multipliers) of, together with the vector tangent to the limit cycle in z_0, that is the eigenvector of the monodromy matrix associated to the Floquet multiplier 1.

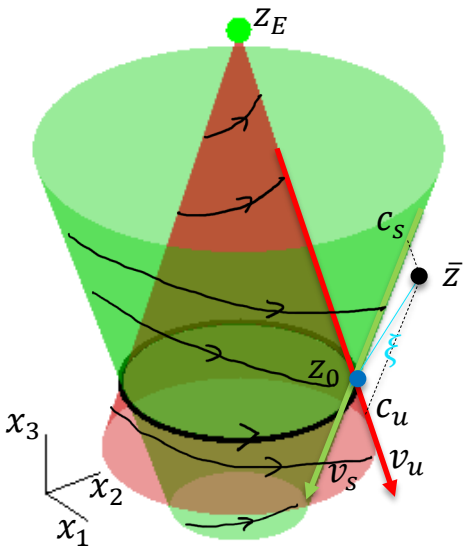

*Figure 9: Phase portrait of a 3D system in the neighborhood of a saddle limit cycle. The stable and unstable manifolds of the limit cycle are shown in green and red, respectively. System trajectories that spiral along the **stable manifold** converge to the limit cycle, while those that spiral along the **unstable manifold** converge to the limit cycle **backward in time**. At a point z_0 on the limit cycle, the eigenvectors of the **monodromy matrix** computed at that point are displayed: v_s (stable) and v_u (unstable). These vectors are tangent to the corresponding manifolds. The **Region of Attraction** of the stable equilibrium z_E is bounded by the stable manifold of the saddle limit cycle: a trajectory starting from an arbitrary initial condition $\bar{z}$ converges to z_E **only if it lies within** the stable manifold of the limit cycle.*

As before, the points that have negative component along the unstable direction, i.e. $c_u < 0$ typically converges to the equilibrium z_E, going elsewhere otherwise. We call this stability criterion **Degree of Stability criterion (DoS criterion).**

Note that the criterion is based on linearization, and therefore make sense to apply it only when we are in the neighborhood of the saddle. Moreover, we need an heuristic to select the point z_0 of the limit cycle on which compute the monodromy matrix.

2.3.1 Applicability of the DoS criterion

The trajectory of car-and-driver during a maneuver is often not close to the limit cycle. If the system is far from the Hopf bifurcation, small disturbances may not bring it near the cycle. On the contrary, large disturbances may cause the driver to lose control before the system feels the influence of the cycle. Even when the trajectory belongs to the stable manifold, some time is needed to approach the cycle. We therefore introduce a **rule to detect when the system is influenced by the cycle**, so that the DoS criterion can be applied meaningfully.

We define a sliding window of length l, storing the **dot product** $DP\left[\bar{z}_0(t_j)\right]$ between the vector field at $\bar{z}_0(t_j)$ and the one at z_0 and the **distance** $D\left[\bar{z}_0(t_j)\right] = \left\|\bar{z}_0(t_j) - z_0\right\|$ computed at the last l time steps. The criterion is applied only if the following holds for all $j = 1, \ldots, l$:

$$DP\left[\bar{z}_0(t_j)\right] > DP_{thr}$$

$$D\left[\bar{z}_0(t_j)\right] < \bar{D}_{thr}$$

Here, D_{thr} is a percentage of the limit cycle amplitude that guarantees closeness, and DP_{thr} ensures collinearity. Including both metrics allows the criterion to apply in a wider range of conditions..

2.3.2 *Selection of the point z_0 on the limit cycle*

To select the point z_0 of the cycle to compute the monodromy matrix, we solve the following **constrained maximization problem**:

$$maximize: (1 - w)DP[\bar{z}_0] + w\left(\frac{D[\bar{z}_0]}{D_{min}}\right)^{-1} \; subject\ to: DP[\bar{z}_0] > 0$$

with:

$$DP[\bar{z}_0] = \frac{(\dot{z}_0 \cdot \dot{z})}{||\dot{z}_0|| \cdot ||\dot{z}||}, \qquad D[\bar{z}_0] = ||z - z_0||, \qquad D_{min} = \min\{D[z_0^i] \; such\ that \; DP[z_0^i] > 0\}.$$

2.3.3 *Practical application*

In Figure , we show two car-and-driver responses to a disturbance during straight motion at $u = 120$ km/h, simulating a wind gust acting on lateral speed v.

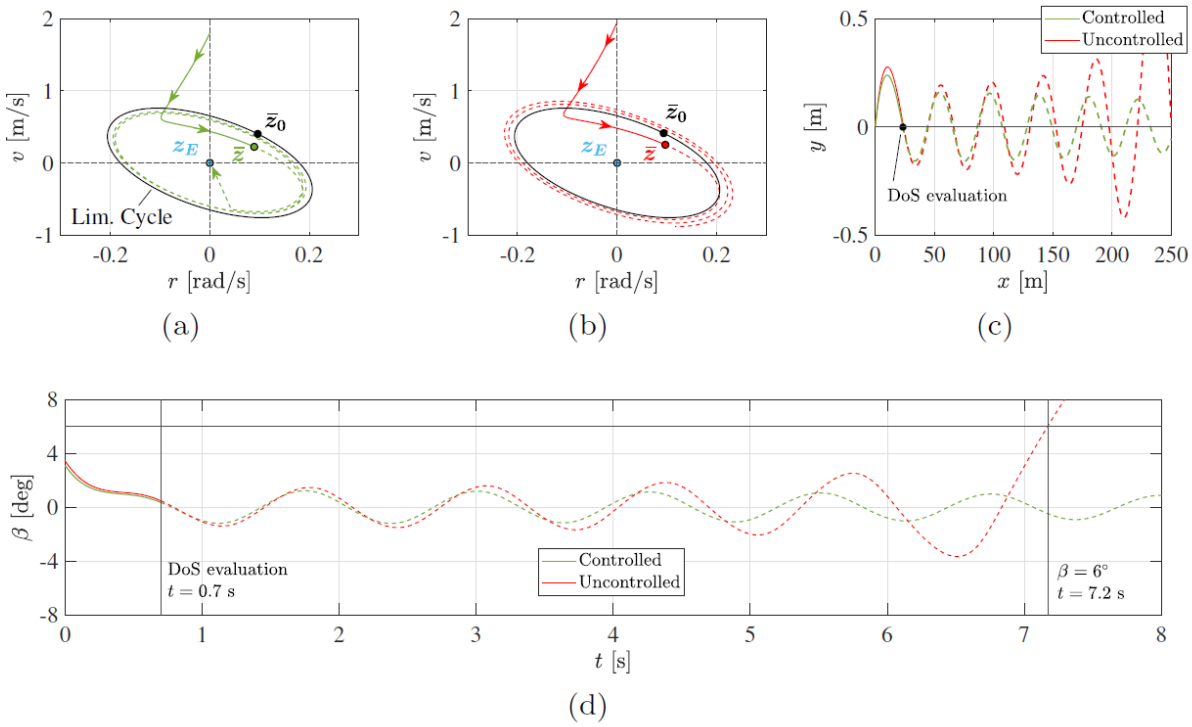

Figure 10: Application of the DoS criterion. (a) the disturbance $(r, v) = \left(0\frac{rad}{s}, 1.8\frac{m}{s}\right)$ excites a controlled straight motion: the system eventually returns to the steady-state condition z_E. The criterion correctly predicts the outcome of the maneuver after $t = 0.7s$ from the application of the disturbance, with stability index $c_u e^{k_u} = 0.087$. (b) the disturbance $(r, v) = \left(0\frac{rad}{s}, 1.95\frac{m}{s}\right)$ excites an uncontrolled motion: the vehicle will spin out. The criterion correctly predicts the outcome of the maneuver after $t = 0.7s$, with stability index $c_u e^{k_u} = -0.1$. (c) trajectory of the vehicle's centre of mass (the reference path is represented as a dotted black line). (d) time history of the vehicle side-slip angle β.

In panel (a) the driver successfully restores the original state. In panel (b) control is lost. In both cases, the DoS criterion predicts the outcome shortly after the disturbance, t=0.7s for straight path, when the side slip

angle β is very small and therefore it is easy to apply a control to react to the disturbance. In panel (d), is reported the common threshold for ESP activation $\beta > 6°$, that would activate control after 7.2s.

2.3.4 Interpretation of the stability index

The coefficient $c_u e^{k_u}$ serves as a **real-time stability index**, which can assist control systems or human drivers to adapt their strategy. This quantitative indicator offers an important advantage over traditional instability detection techniques. Even when maneuvers are technically "recovered", they may feature strong oscillations and thus be considered unsafe. This is captured by small values of $c_u e^{k_u}$, indicating proximity to the saddle manifold and thus marginal stability.

3 Method to introduce Lyapunov functions into complex vehicle models

A mathematical tool that, thanks to the La Salle principle, allows a formal estimation of regions all contained in the stability region, also called in this context **Region of Attraction** (ROA) is the Lyapunov function. For the model we presented, we have proposed a kinetic energy-based Lyapunov function, with the idea that if a disturbance is absorbed by the system the kinetic energy of the system vanishes, while if is cause instability it diverges.

3.1 Formal definition of a Lyapunov function for vehicle dynamics

To analyze the response of a vehicle-and-driver system to disturbances, we introduce a Lyapunov function V whose time derivative is defined as:

$$\dot{V} = -(\Delta E_{\mathrm{k}} + E_{\mathrm{s}}),$$

where ΔE_{k} is the variation in kinetic energy due to the vehicle's motion, and E_{s} is the energy associated with the steering action.
The kinetic energy variation, derived using König's theorem, includes both translational and rotational components, and is expressed as:

$$\Delta E_{\mathrm{k}} = (1/2)\, m\, v^2 + (1/2)\, J\, r^2,$$

assuming constant forward velocity u and an initial steady-state condition $v(0) = r(0) = 0$.

Note that ΔE_{k} is the result of the work done by all active forces acting on the system:

$$\Delta E_{\mathrm{k}} = \int_0^{y_f} F_{y_f}\, dy_f + \int_0^{y_r} F_{y_r}\, dy_r + \int_0^{t} mvr\, dt + \int_0^{y_G} F\, dy_G + \int_0^{\varphi} M\, d\psi,$$

where:

- F_{y_f}, F_{y_r} are lateral tire forces at the front and rear axles;
- mvr is the inertial longitudinal force required to maintain constant forward velocity;
- F and M are external disturbance force and moment applied to the vehicle body;

and therefore it contains all the information on all of the acting forces and all of the state variables, and is thus a meaningful quantity.
The energy associated with the driver's steering action E_{s} accounts for internal elastic, viscous, and inertial torques:

$$E_{\mathrm{s}} = \int_0^{\delta} \xi\, \delta\, d\delta + \int_0^{\delta} \xi\, \tau\, \delta\, d\delta + \int_0^{\delta} \xi\, \tau^2 \delta\, d\delta,$$

but is found to be several orders of magnitude smaller than ΔE_{k}, and thus negligible for the purposes of Lyapunov analysis.
The resulting expression for the Lyapunov function derivative becomes:

$$\dot{V} \approx -((1/2)\, m\, v^2 + (1/2)\, J\, r^2),$$

which is negative definite for all $v, r \neq 0$.
By applying the fundamental theorem of integral calculus we therefore get

$$V(t) - V(x(0)) \approx \int_0^{t} -\left(\frac{1}{2}\, m\, v^2 + \frac{1}{2}\, J\, r^2\right) dt$$

and therefore, if we are in the ROA of 0 (and therefore $\lim_{t\to\infty} V(t) = 0$) the Lyapunov function is

$$V(x(0)) \approx \int_0^{t} \left(\frac{1}{2}\, m\, v^2 + \frac{1}{2}\, J\, r^2\right) dt$$

This leads to a necessary and sufficient condition for post-disturbance recovery:

$$\lim_{t\to\infty} \Delta E_{\mathrm{k}}(t) = 0 \Leftrightarrow \lim_{t\to\infty} v(t) = r(t) = 0\,.$$

Although theoretically rigorous, this formulation requires full knowledge of the system trajectory to compute $V(x)$, making it unsuitable for a priori estimation of the ROA. For this reason, the next section

introduces an SOS-based approach for constructing a Lyapunov function that enables ROA estimation via polynomial optimization.

3.2 Sum Of Squares (SOS) methods to inner approximate of the stability region

Given a dynamic system $\dot{x} = f(x)$ with a fixed point at the origin, a Lyapunov function $V(x)$ is a scalar, energy-like scalar function that satisfies the following properties: $V(x)$ is positive definite, and its Lie derivative along the system dynamics $\dot{V}(x) = \frac{\partial V(x)}{\partial x} f(x)$ is a negative semi-definite function. Finding a Lyapunov function proves that the fixed point at the origin is a stable equilibrium (Lyapunov's Direct Method). If $\dot{V}(x)$ is negative definite (a stricter condition), this further implies asymptotic stability. While the size of the region where these definiteness conditions hold is not relevant to characterize the equilibrium, it is essential to estimate the ROA.

A sublevel set $S = \{x: V(x) < \rho\}$ on which $\dot{V}(x) \leq 0$ is an invariant set for the system, i.e., trajectories starting from $\overline{x} \in S$ always remain inside S. According to LaSalle's theorem, these trajectories converge to the largest invariant subset of S where $\dot{V}(x) = 0$. If that subset consists of the origin alone, then S is an inner approximation of its ROA. The practical challenge is to find a Lyapunov function that leads to the largest possible sublevel set S satisfying these properties.

To address this, **sum-of-squares (SOS)** methods provide a computational framework for constructing Lyapunov functions and estimating ROA in systems with **polynomial dynamics**. A polynomial is SOS if it can be written as the sum of the squares of other polynomials. This guarantees that it is globally positive semi-definite. The key advantage is the SOS condition can be enforced efficiently as convex constraint in **semidefinite programs (SDP)**.

We first illustrate the approach on a benchmark system, the **time-reversed Van der Pol oscillator**. This system already has polynomial dynamics and has an asymptotically stable equilibrium at the origin. Its ROA is known and corresponds with the region within the unstable limit cycle. Our aim is to efficiently approximate the ROA as a level set of a polynomial Lyapunov function. Several software packages are available to solve SOS problems; we utilized Drake Python toolbox developed at MIT with Mosek solver.

First, we compute a polynomial Lyapunov function $V(x)$ of fixed degree for e linearized system around the origin. To achieve this, it is sufficient to solve a feasibility SDP problem with SOS constraints $V(x)$ and on $-\dot{V_{lin}}(x) = -\frac{\partial V(x)}{\partial x}\frac{\partial f(x)}{\partial x}x$. Additional linear constraints as $V(0) = 0$ are required for positive definiteness. The obtained Lyapunov function is the starting point for the following three step iterative procedure we propose.

1. Given a Lyapunov function $V(x)$, we find the maximum level value ρ for which the corresponding level set is within the region where $\dot{V}(x) < 0$ (fig. 1a). This step is based on the **S-procedure**, which introduces a polynomial multiplier $\lambda(x)$ to prove the region inclusions.
2. Given the Lyapunov level set found in step 1, we find the largest ellipse $x^T P x = 1$ within the level set (fig. 1b). This step is also based on the S-procedure and introduces a second polynomial multiplier $\mu(x)$.
3. Given the two multipliers found in steps 1 and 2, we search for a new Lyapunov function by maximizing the area of the ellipse contained within the Lyapunov level set. (fig. 1c) Formally, the constraints of this SDP problem are the same of the previous steps, but now the multipliers are fixed, while the coefficients of the Lyapunov function $V(x)$ and the inner ellipse matrix P are decision variables.

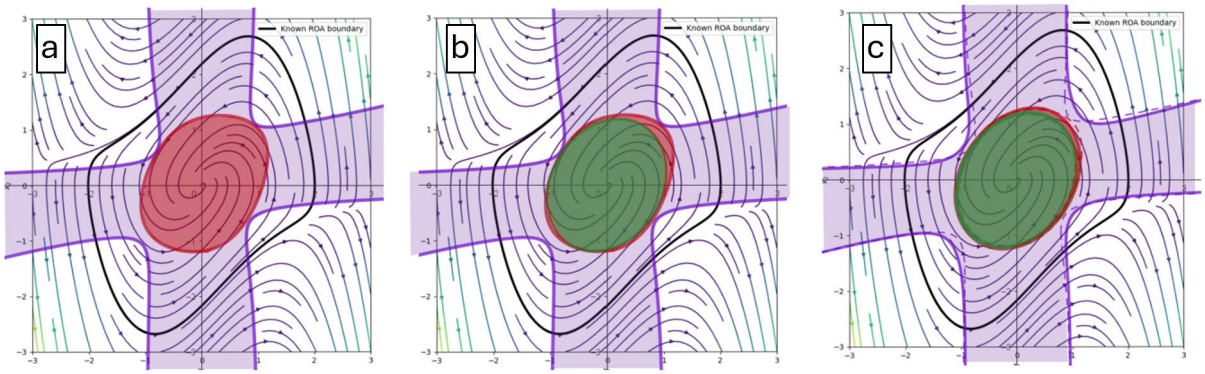

Figure 11: Steps of the procedure

By adopting the described procedure with a 6-th degree Lyapunov function, it is possible to obtain a tight approximation of the time-reversed Van der Pol ROA in only 7 iterations. The result is shown in Figure 11. The result is shown in the left panel of Figure 12.

An even more compelling aspect concerns the determination of a subset of the ROA for which it is guaranteed that all trajectories starting from within remain inside prescribed bounds throughout their evolution. By incorporating such requirements as additional SOS constraints in the previous optimization steps, we can compute an inner approximation of the ROA that is also an invariant set and that complies with the specified bound constraints. This approach is particularly relevant in safety-critical applications, where constraints on the state variables must be always satisfied and not only asymptotically. An illustrative example is reported in the right panel of Figure 12 for the time-reversed Van der Pol system, where the constraint $x_1^2 \leq 1$ must be satisfied throughout the trajectory.

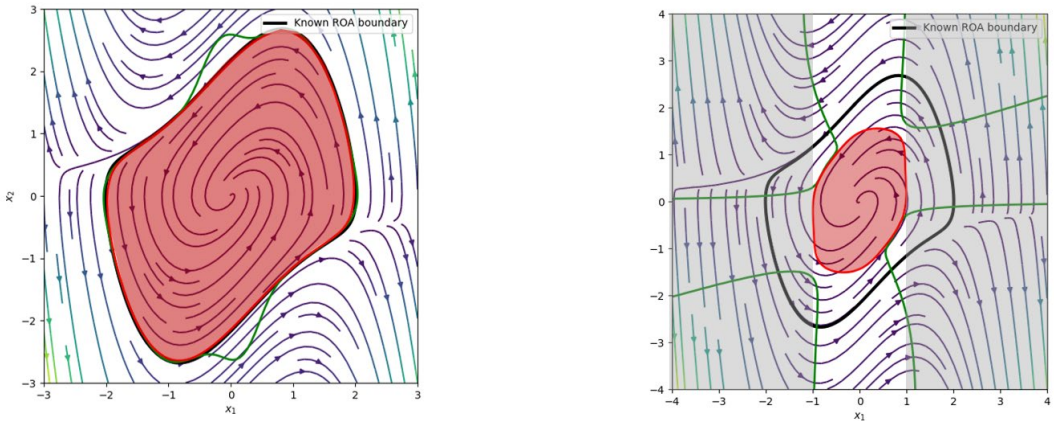

Figure 12: RoA approximation with a 6-th degree Lyapunov function without (left panel) and with (right panel) state constraints

The main challenges in applying the described procedure to vehicle-with-driver systems are the following:

- the need for a **polynomial approximation** of the system dynamics
- a **larger number of state variables**, typically greater than six

Concerning the first point, the primary source of non-polynomial nonlinearity lies in the **tire constitutive equations**. Even simplified versions of the well-known Magic Formula require a high-degree polynomial

for accurate fitting. Both the degree of the approximating polynomial dynamics and the number of state variables heavily affect the size of the resulting Semidefinite Programming (SDP) problems, since the decision variables correspond to the coefficients of the SOS polynomial to be identified. A polynomial of degree d in m variables may contain up to $\frac{(m+d)!}{m!\,d!}$ monomials, leading to a combinatorial growth in complexity.

To address this issue, one may leverage **state constraints** to restrict the dynamics within a meaningful operating range. For example, imposing an upper bound on the magnitude of **tire slip angles** serves a twofold purpose: it ensures that the system evolves within a physically plausible region, and at the same time it enables a lower-degree polynomial approximation of the tire behavior, such as a cubic fit, within that region—thus avoiding the saturation zones.

The application of the described methods to vehicle-with-driver models is currently under development. Preliminary results are promising and will be presented in future contributions.

3.Path tracking for motorsport and road vehicles

Traditional planning methods in high-performance racing contexts often operate at the edge of physical constraints (e.g., tire grip or track limits) but typically neglect the explicit modeling of disturbances or uncertainties. As a result, even small deviations during execution can lead to constraint violations and unsafe behavior. Our work focuses on enhancing trajectory planning for motorsport vehicles by incorporating uncertainty directly into the planning stage, aiming to achieve both minimum lap time and probabilistic safety guarantees.

The mathematical framework is built upon a **nonlinear stochastic dynamic model** of a race vehicle. The nominal vehicle dynamics is described using a **single-track model** with nonlinear tire characteristics, with longitudinal force and steering angle as control inputs $\boldsymbol{u}(t)$. To model real-world uncertainties (such as sensor noise or unmodeled dynamics), we add a **noise term** $\boldsymbol{w}(t)$ to the dynamics.

$$\dot{\boldsymbol{x}}(t) = f\big(\boldsymbol{x}(t), \boldsymbol{u}(t)\big) + \boldsymbol{w}(t)$$

The vehicle state $\boldsymbol{x}(t)$ is modeled as a **Gaußian random variable** characterized by a time-varying **mean** $\boldsymbol{\mu}(t)$ and **covariance matrix** $\boldsymbol{P}(t)$. The evolution of the mean follows the standard deterministic dynamics, while the covariance evolves through a **Lyapunov differential equation**, which depends on the system's Jacobian evaluated along the mean trajectory:

$$\dot{\boldsymbol{\mu}}(t) = f\big(\boldsymbol{\mu}(t), \boldsymbol{u}(t)\big)$$

$$\dot{\boldsymbol{P}}(t) = \boldsymbol{A}(t)\,\boldsymbol{P}(t) + \boldsymbol{P}(t)\,\boldsymbol{A}^{T}(t) + \boldsymbol{Q}(t)$$

where $\boldsymbol{Q}(t)$ is the covariance matrix associated with the noise $\boldsymbol{w}(t)$.

This formulation enables the use of **probabilistic constraints;** each system constraint (e.g., tire force limits or track boundaries) is reformulated by introducing a **back-off term**, based on a linearization of the constraint. This term depends on the covariance $\boldsymbol{P}$ and the desired confidence level to fulfill the requirements. This ensures that the constraint is satisfied with a user-defined probability (e.g., 90%, 99%). The resulting **optimal control problem** is discretized via **direct collocation** and solved using interior point method, thereby simultaneously optimizing the mean trajectory, the control inputs, and the evolution of the covariance.

The study introduces two complementary planning strategies that explicitly account for disturbances.

1. **Open-Loop Worst-Case Covariance Propagation.** This method propagates the vehicle's state covariance forward over a fixed **prediction horizon** at each discretization step. Constraints are tightened based on the uncertainty at the end point of the prediction horizon, without considering any feedback action during planning. Although conservative, this approach improves robustness by ensuring that the planned trajectory meets the constraints with the desired probability along the whole evolution.

2. **Closed-Loop Covariance-Aware Planning.** This more sophisticated approach incorporates into the planning process a time-varying **feedback controller** based on a Linear Quadratic Regulator (LQR). It starts by computing a nominal minimum-time trajectory assuming deterministic dynamics. Then, an LQR controller is designed to stabilize that trajectory. Finally, the planning problem is re-solved with both the trajectory and controller gains as decision variables, ensuring

that the planned trajectory remains robust under closed-loop uncertainty propagation. This enables more realistic and less conservative behavior, as it exploits the stabilizing action of feedback.

A comprehensive simulation study is conducted on a section of the Catalunya racing circuit. The analysis investigates the influence of key parameters, such as initial uncertainty and desired safety levels (Figure 13), on the resulting trajectories. The impact of each robustified constraint (track limits, friction limits, or both) is examined to understand how different safety requirements shape the driving strategy, including acceleration and braking force profiles and steering inputs. A comparison between Open-Loop and Closed-Loop strategies is shown in Figure 14. The highlighted regions illustrate how the vehicle's safety envelope changes over time due to probabilistic constraint tightening. It is worth noting that the Open-Loop strategy gives more conservative results.

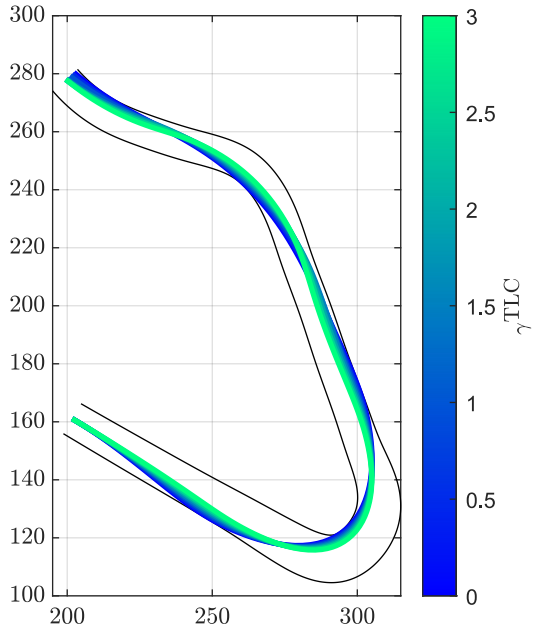

Figure 13: Dependence of planned trajectories on the required confidence level for Track Limits Constraints (TLC). Higher values of γ^TLC correspond to higher confidence levels.

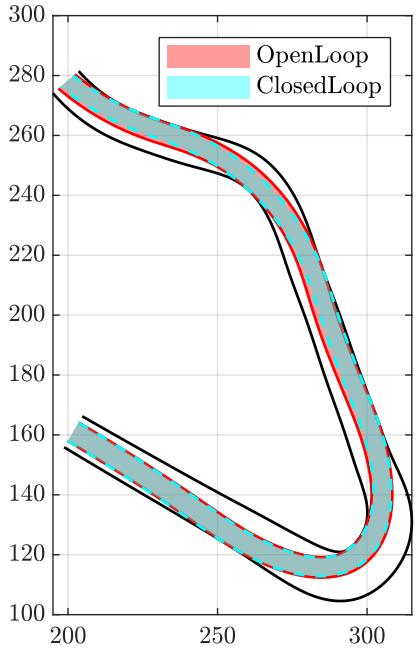

Figure 14: Comparison between vehicle's safety envelopes obtained via Open-Loop and Closed-Loop strategies with Track Limits Constraints (TLC).

In conclusion, this work provides a novel contribution to robust trajectory planning in motorsport by integrating probabilistic safety guarantees and feedback-aware planning. The results suggest that it is possible to achieve high-performance lap-time optimization without compromising safety, even in the presence of significant disturbances, and will be detailed in a forthcoming publication currently in preparation.

Conclusions

Referring to the scheduled activities, the following topics had to addressed

-Bifurcation Analysis

-Taxonomy of bifurcations

-Lyapunof function investigation

-Path tracking for motorsport and road vehicles

All of the topics have been tackled with original results.

-Bifurcation Analysis: The drivers introduces bifurcations, we have understood the pattern of stable or unstable motion of any driver as a consequence of a disturb. Form now on engineers will have an additional way of interpreting telemetry. Trajectories in the phase plain will be always conditioned by the presence of a limit cycle.

-Taxonomy of bifurcations: Due to the presence of limit cycles, a taxonomy has been performed easily, actually it coincides with the taxonomy of limit cycles

-Lyapunof function investigation: We have shown that the problem of instability depends on the rotational kinetic energy that leaks from the translational kinetic energy by means of the inertia forces.

-Path tracking for motorsport and road vehicles: We have demonstrated that high-performance trajectory planning in motorsport can effectively integrate uncertainty, with or without a feedback controller, enabling minimum lap-time strategies that are both fast and probabilistically safe.

References

[1] Pacejka, H.B., Tyre and Vehicle Dynamics. Butterworth and Heinemann (also SAE). Oxford, U.K., 2002, 2nd edn., 2006; 3ed., 2013
[2] Kuznetsov, Y. A., Kuznetsov, I. A., & Kuznetsov, Y. (1998). *Elements of applied bifurcation theory* (Vol. 112, pp. xx+-591). New York: Springer.
[3] Mastinu, G., Della Rossa, F., Previati, G. et al. Global stability of road vehicle motion with driver control. Nonlinear Dyn 111, 18043–18059 (2023). https://doi.org/10.1007/s11071-023-08794-z
[4] https://www.vi-grade.com/, retrieved May 2025.
[5] Praolini, F., Bifurcation analysis of a torque vectoring control system for a road vehicle, Master thesis, AA 2023/2024, https://www.politesi.polimi.it/handle/10589/235242
[6] Mastinu G, Previati G, Della Rossa F, Gobbi M, Fainello M, "How Drivers Lose Control of the Car", SAE International Journal of Vehicle Dynamics, Stability, and NVH, 2024
[7] Giacintucci, S., Della Rossa, F., & Mastinu, G. (2025). Early detection of unstable car-and-driver motion—a Floquet theory approach. *Nonlinear Dynamics*, 1-20.